*Journal of Sound and Vibration* (2002) **251**(2), 349–366
doi:10.1006/jsvi.2001.4008, available online at http://www.idealibrary.com on IDEAL®

# ANALYSIS OF SOUND TRANSMISSION THROUGH PERIODICALLY STIFFENED PANELS BY SPACE-HARMONIC EXPANSION METHOD

J.-H. Lee and J. Kim

*Structural Dynamics Research Laboratory, Mechanical Engineering Department, University of Cincinnati, Cincinnati, OH* 45221-0072, *U.S.A. E-mail: jay.kim@uc.edu*

(*Received* 26 *February* 2001, *and in final form* 4 *September* 2001)

An analysis method is developed to study sound transmission characteristics of a thin plate stiffened by equally spaced line stiffeners. The dynamic equation that describes the vibro-acoustic response of the system is derived by expanding the structural and acoustic responses in terms of the space harmonics and by using the virtual energy method. The series solution can be considered as the exact solution because the structural and acoustic–structural coupling effects in the system are fully considered and the solution converges. Parameter studies are conducted for major design parameters to understand the characteristics of the system.



## 1. INTRODUCTION

### 1.1. OVERVIEW OF THE WORK

Thin plates stiffened by parallel, equally spaced line stiffeners are commonly found in aircraft and marine structures. In the low-frequency range in which the wavelength of the flexural wave in the plate is much longer than the stiffener spacing, such a structure can be modelled as an orthotropic plate. At a relatively high frequency, at which the flexural wavelength is comparable with stiffener spacing, the structure has to be modelled as a panel with a periodically deployed stiffener. The structural response of the periodic structure to harmonic excitations has been obtained by expanding it in terms of a series of space harmonics by Mead *et al.* [1–3] to investigate structural responses of periodically stiffened beams and plates. This approach is also adopted in this work to solve the vibro-acoustic equation of the stiffened plate subjected to a plane wave input to calculate the transmission loss (TL) through the structure. In the work by Mead *et al.*, acoustic responses were obtained based on the uncoupled model assuming that acoustic pressure excites the structure, but the structural response does not induce further acoustic responses. Therefore, the TL cannot be calculated by the uncoupled approach.

If a panel is stiffened only in one direction, the two-dimensional, periodically stiffened panel may be modelled as a one-dimensional structure, essentially a periodically supported beam as illustrated in Figure 1. The stiffener can be represented as a combination of a lumped mass ($M$), rotational ($K_r$) and translational ($K_t$) springs as shown in Figure 1. An experimental or numerical method may be used to determine the spring rates. For example, an FE analysis may be used to obtain the ratios between the force and the displacement, which may be used as the linear spring rate.

0022-460X/02/120349 + 18 $35.00/0 

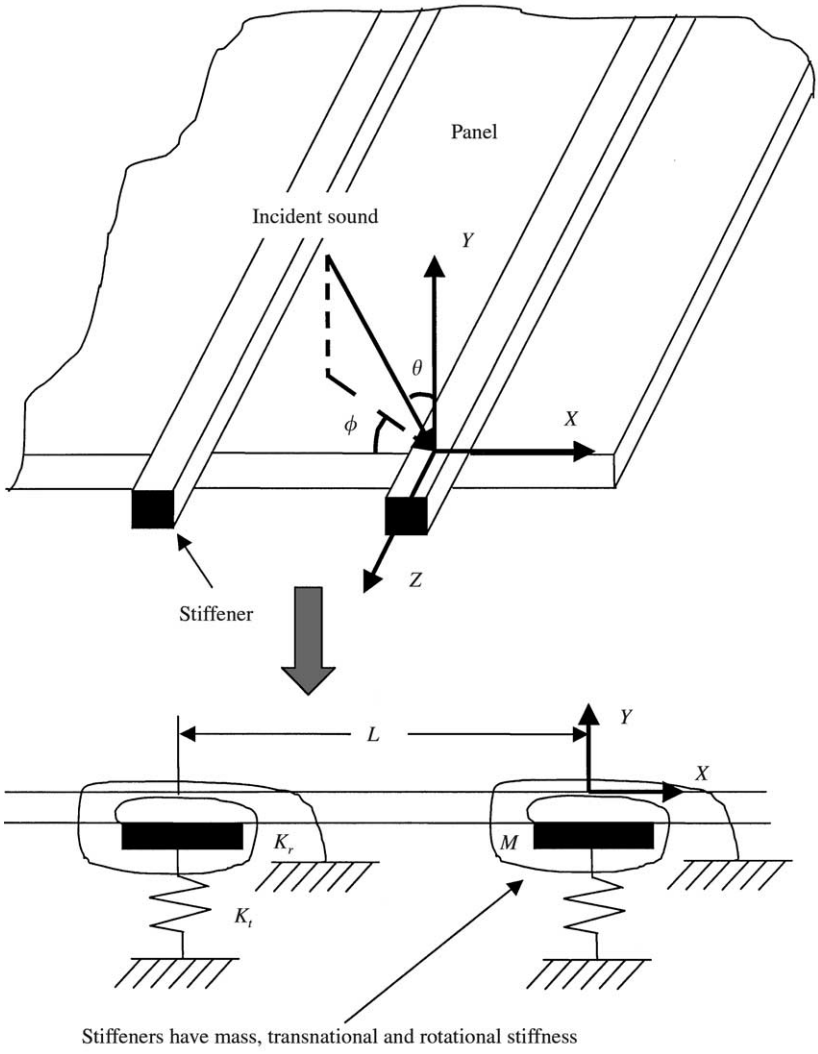


Figure 1. Schematic representation of a stiffened panel.

The system equation is developed by combining the wave equations in the incident and transmitted side, the beam equation representing the plate and the effect of the lumped mass and springs representing the stiffener, which are coupled with one another. A unique analysis technique is developed to solve this vibro-acoustically coupled problem. Utilizing the analysis result, characteristics of the sound transmission through a periodically stiffened plate are studied with special attention to the role of the stiffener in the sound transmission. The analysis procedure developed in this work, which is based on the space harmonic method could be obviously extended to other types of structures. For example, sound transmission characteristics through a cylindrical shell with a periodic ring stiffener are being studied by the authors using the approach in their concurrent work.

### 1.2. RELATED LITERATURE

The response of stiffened plates excited by random pressure fields can be obtained by the normal mode expansion method [4–7]. Because the normal modes of the stiffened plates

must be determined, the method is confined to systems with relatively simple boundary conditions. The structural wave propagation in periodically supported, undamped beams and grillages was studied by Heckl [8]. It was shown that flexural waves can propagate freely (without rapidly decaying) only in certain frequency bands. If the periodic structure is highly damped, a wave approach yields the response much more readily as demonstrated by Mead and Wilby [9]. A relatively simple formula was developed for the displacement, curvature or stress at any point in the beam.

Mead and Pujara [1] developed a space harmonic method, in which the system response is expended in terms of the harmonics of the stiffener spacing. This method is attractive because the sound radiation effects can be very easily incorporated as the transverse dispalcement can be expressed as a series of sinusoidal travelling waves. In their work, the panel is represented as a beam supported at regular intervals on elastic constraints that oppose both transverse displacements and flexural slope changes. The response of the beam subjected to a homogeneous random convected pressure field was solved, in which the coupling between the acoustic system and the structural system is not considered (acoustic pressure acts as structural excitation, but the effect of the structural response on the acoustic system is not included). Structural responses of two-dimensional plates with orthogonal stiffening were investigated by Lin [5, 6], Mercer [7], Ford [10] and Mercer and Seavey [11] assuming that the plate is simply supported in one direction.

Sound transmission problems were studied by some researchers, which however are incomplete work [12] or are limited to low frequencies due to the related simplifications [13]. Mathur *et al.* [12] proposed a theoretical model based on the space harmonic approach to calculate the transmission loss through a periodically stiffened panel and stiffened double-panel structures, however, without showing any numerical results. Schemes to impose the structure–acoustic interactions and convergence of the solution are developed in this work to make the space harmonic method work for these types of problems. Desmet *et al.* [13] presented a method to find the sound transmission properties of finite double-panel partitions as low frequencies by adopting an experimental approach as well as a theoretical method based on Dowell's modal coupling theory [14].

Bedair [15] and Molaghasemi [16] investigated the dynamic behavior (e.g., the fundamental frequency of stiffened plates) of plates stiffened by a system of interconnected beams or ribs. Wei *et al.* [17, 18] discussed the application of the Rayleigh–Ritz and extended Rayleigh–Ritz energy methods to finite periodic structures with sinusoidal displacement functions and also studied the relations between his method for analyzing finite periodic structures and the theory of infinite periodic structures.

## 2. FORMULATION OF THE SYSTEM EQUATION

Figure 1 illustrates the system to be studied, which is a typical set-up that defines the transmission loss. A plane wave is incident to a flat panel with a periodic stiffener, which induces the reflected wave, the panel motion, and the transmitted wave. The transmitted side is assumed to be anechoic, therefore there is no reflected wave on the transmitted side.

Because of the periodic nature of the system, the system responses are also expected to be periodic. Therefore, the transverse motion of the panel in Figure 1 can be expressed as a series of space harmonics [1], i.e.:

$$W(x, t) = \sum_{n=-\infty}^{+\infty} A_n \, \mathrm{e}^{-\mathrm{j}[(\mu + 2n\pi)/L]x} \, \mathrm{e}^{\mathrm{j}\omega t}, \tag{1}$$

where $W(x, t)$ is the panel transverse displacement, coefficients $A_n$ can be considered as modal amplitudes of the structure, $L$ is the spacing between stiffeners, and $\mu$ is the characteristic propagation constant which is defined as

$$\frac{\mu}{L} = k_x(\omega) - \mathrm{j}\psi(\omega), \tag{2}$$

where $\omega$ is the angular frequency, $\psi$ is the phase attenuation coefficient and $k_x$ is the component of the wave number along the $x$-axis. Refering to Figure 1, component wave numbers $k_x$ and $k_y$ can be obtained as

$$k_x = k \sin\theta \cos\phi, \quad k_z = k \sin\theta \sin\phi, \tag{3, 4}$$

where $k = \omega/c$ is the wave number of the incident plane wave, $c$ is the speed of sound, $\theta$ and $\phi$ are the incidence angles of the plane wave in the $x$–$y$ plane and $x$–$z$ plane. The plane wave is assumed to be incident along $X$–$Y$ plane, thus, i.e., $\phi = 0$ in this study. Non-zero $\phi$ cases, which require a two-dimensional description for the panel wave in equation (1), are being studied currently by the authors.

Notice that in equation (1) the structural wave is expressed as the sum of space harmonics corresponding to $n = 0, \pm 1, \pm 2, \pm 3, \ldots$, for the forward as well as backward waves, which represent reflections at the stiffener joint. Each of the space harmonic does not satisfy the boundary condition, however, their sum is forced to satisfy the boundary condition.

The velocity potential at a point in the incident side half space is composed of the potentials of the incident and reflected waves. The reflected wave is also expected to be periodic spatially; the wave velocity potential $\Phi_1(x, y, t)$ is represented as

$$\Phi_1(x, y, t) = \mathrm{e}^{-\mathrm{j}((\mu/L)x + k_{y0}y - \omega t)} + \sum_{n=-\infty}^{+\infty} B_n \mathrm{e}^{-\mathrm{j}([(\mu + 2n\pi)/L]x - k_{yn}y - \omega t)}, \tag{5}$$

where the first term represents the potential of the incident wave and the second term in a series form represents that of the reflected wave. $\Phi_2(x, y, t)$, the velocity potential of the transmitted wave, is also spatially periodic, therefore expressed as

$$\Phi_2(x, y, t) = \sum_{n=-\infty}^{+\infty} C_n \mathrm{e}^{-\mathrm{j}([(\mu + 2n\pi)/L]x + k_{yn}y - \omega t)}. \tag{6}$$

In equations (5) and (6), $k_{yn}$ is the wave number in the $y$ direction, which can be obtained from the relationship

$$k_{yn} = \sqrt{\left(\frac{\omega}{c}\right)^2 - \left(\frac{\mu + 2n\pi}{L}\right)^2 - k_z^2}. \tag{7}$$

Coefficients $B_n$ and $C_n$ may be considered as modal amplitudes of the reflected and transmitted waves.

The modal amplitudes of the reflected and transmitted waves can be related to those of the structural wave by considering the boundary condition of the normal velocities [19]. At $y = 0$:

$$-\frac{\partial \Phi_1}{\partial y} = \mathrm{j}\omega W, \qquad -\frac{\partial \Phi_2}{\partial y} = \mathrm{j}\omega W. \tag{8, 9}$$

By substituting equations (1), (5) and (6) into equations (8) and (9), we obtain

$$\omega \sum_{n=-\infty}^{\infty} A_n e^{-[(\mu+2n\pi)/L]x} + \sum_{n=-\infty}^{+\infty} k_{yn} B_n e^{-[(\mu+2n\pi)/L]x} - k_{y0} e^{-(\mu/L)x} = 0, \tag{10}$$

$$\omega \sum_{n=-\infty}^{\infty} A_n e^{-[(\mu+2n\pi)/L]x} - \sum_{n=-\infty}^{+\infty} k_{yn} C_n e^{-[(\mu+2n\pi)/L]x} = 0. \tag{11}$$

Because equations (10) and (11) should be valid at all values of $x$, the relationships between the modal amplitudes are obtained. From equation (10),

$$B_n = 1 - \omega \frac{A_n}{k_{yn}}, \quad \text{when } n = 0, \qquad B_n = -\omega \frac{A_n}{k_{yn}}, \quad \text{when } n \neq 0. \tag{12a, b}$$

From equation (11),

$$C_n = \omega \frac{A_n}{k_{yn}}. \tag{13}$$

Therefore, if the coefficients $A_n$, modal amplitudes of the flexural wave in the panel, are found, all other coefficients are also found. The coefficients $A_n$ can be found by solving the system equation, which is derived by applying the principle of virtual work for one period of the beam as proposed by Mead [1]. The principle states that the sum of the works done by all elements in one period of the system must do no work when the system moves through any one of the virtual displacements:

$$\delta W = \delta A_m e^{-j([(\mu+2m\pi)/L]x - \omega t)}. \tag{14}$$

The virtual work of one period of a panel element is calculated at first. The equation of motion of the beam representing the unit depth of the panel is [20]

$$D \frac{d^4 W}{dx^4} - m_p \omega^2 W - j\omega \rho_0 (\Phi_1 - \Phi_2) = 0, \tag{15}$$

where $m_p$ is the panel mass per unit length and $\rho_0$ is the density of air, and $D$ is the flexural stiffness of the panel defined as [20]

$$D = \frac{Eh^3}{12(1-\nu^2)}, \tag{16a}$$

where $h$ is the panel thickness, $E$ and $\nu$ are the *in vacuo* Young's modulus and the Poisson ratio of the panel material. If necessary, structural damping of the panel material can be introduced by taking $D$ as

$$D = \frac{Eh^3}{12(1-\nu^2)}(1 + j\eta), \tag{16b}$$

where $\eta$ is the loss factor of the beam material [21]. The structural loss factor $\eta$ and the phase attenuation coefficient $\psi(\omega)$ in equation (2) are closely related; however, they have to be estimated separately by experiments because other conditions or parameters such as geometric discontinuity also influence the latter. The last term in equation (15) represents the acoustic and structural coupling effect. In equation (5), the equivalent force is applied to

a unit length of the beam. Thus, the virtual work contributed by the panel can be represented as

$$\delta\Pi_p = \int_{x=0}^{L} \left( D\frac{\mathrm{d}^4 W}{\mathrm{d}x^4} - m_p\omega^2 W - \mathrm{j}\omega\rho_0(\Phi_1 - \Phi_2) \right)\delta W^*, \tag{17}$$

where $\delta W^*$ represents the complex conjugate of the virtual displacement in equation (14). Therefore, by substituting equations (5) and (6) into equation (17), the virtual work done by the panel is obtained as

$$\begin{aligned}\delta\Pi_p = \delta A_m^* \Bigg\{ & \int_0^L D \sum_{n=-\infty}^{\infty} \left(\frac{\mu + 2n\pi}{L}\right)^4 A_n \mathrm{e}^{-\mathrm{j}[(\mu+2n\pi)/L]x} \mathrm{e}^{\mathrm{j}[(\mu+2m\pi)/L]x}\,\mathrm{d}x \\ & - \int_0^L \sum_{n=-\infty}^{\infty} m_p\omega^2 A_n \mathrm{e}^{-\mathrm{j}[(\mu+2n\pi)/L]x} \mathrm{e}^{\mathrm{j}[(\mu+2m\pi)/L]x}\,\mathrm{d}x \\ & - \int_0^L \mathrm{j}\omega\rho_0 \Bigg[ \mathrm{e}^{-\mathrm{j}(\mu/L)x} \mathrm{e}^{-\mathrm{j}k_{y0}y} \mathrm{e}^{\mathrm{j}[(\mu+2m\pi)/L]x} + \sum_{n=-\infty}^{\infty} B_n \mathrm{e}^{\mathrm{j}k_{yn}y} \mathrm{e}^{-\mathrm{j}[(\mu+2n\pi)/L]x} \mathrm{e}^{\mathrm{j}[(\mu+2m\pi)/L]x} \\ & - \sum_{n=-\infty}^{\infty} C_n \mathrm{e}^{-\mathrm{j}[(\mu+2n\pi)/L]x} \mathrm{e}^{-\mathrm{j}[(\mu+2m\pi)/L]x} \mathrm{e}^{-\mathrm{j}k_{yn}y} \Bigg]\mathrm{d}x \Bigg\}. \end{aligned} \tag{18}$$

The contribution to the virtual work by the translational spring is equal to

$$\delta\Pi_t = K_t W(0)\,\delta A_m^* = \delta A_m^* K_t \sum_{n=-\infty}^{\infty} A_n. \tag{19}$$

The contribution to the virtual work by the rotational spring per one period of the system is equal to

$$\delta\Pi_r = \mathrm{j}K_r W'(0)\delta A_m^* \left(\frac{\mu + 2m\pi}{L}\right) = \delta A_m^* K_r \sum_{n=-\infty}^{\infty} A_n \left(\frac{\mu + 2n\pi}{L}\right)\left(\frac{\mu + 2m\pi}{L}\right). \tag{20}$$

The contribution of the lumped mass to the virtual work per one period of the system becomes

$$\delta\Pi_M = -\omega^2 M W(0)\,\delta A_m^* = -\omega^2 M \delta A_m^* \sum_{n=-\infty}^{\infty} A_n. \tag{21}$$

Finally, the virtual work principle requires that

$$\delta\Pi_p + \delta\Pi_t + \delta\Pi_r + \delta\Pi_M = 0. \tag{22}$$

Evaluating the integrals involved in $\delta\Pi_p$ and noticing that the virtual displacement is arbitrary, equation (22) results in the following equation:

$$\begin{aligned} & \left[ D\left(\frac{\mu + 2m\pi}{L}\right)^4 - m_p\omega^2 \right] A_m + \left(\frac{K_t}{L} - \frac{\omega^2 M}{L}\right) \sum_{n=-\infty}^{\infty} A_n + \frac{K_r}{L} \sum_{n=-\infty}^{\infty} A_n \left(\frac{\mu + 2n\pi}{L}\right)\left(\frac{\mu + 2m\pi}{L}\right) \\ & = \mathrm{j}\omega\rho_0[B_m - C_m + 1], \quad \text{when } m = 0, \end{aligned} \tag{23a}$$

$$= \mathrm{j}\omega\rho_0[B_m - C_m], \quad \text{when } m \neq 0. \tag{23b}$$

On substituting the relationships between the modal amplitudes defined in equations (12) and (13), equation (23) becomes

$$\left[D\left(\frac{\mu+2m\pi}{L}\right)^4 - m_p\omega^2 + \frac{2\rho_0\omega^2 \mathrm{j}}{k_{ym}}\right]A_m + \left(\frac{K_t}{L} - \frac{\omega^2 M}{L}\right)\sum_{n=-\infty}^{\infty} A_n + \frac{K_r}{L}\sum_{n=-\infty}^{\infty} A_n\left(\frac{\mu+2n\pi}{L}\right)\left(\frac{\mu+2m\pi}{L}\right)$$

$$= 2\omega\rho_0 \mathrm{j}, \quad \text{for } m = 0, \tag{24a}$$

$$= 0, \quad \text{for } m = \pm 1, \pm 2, \pm 3, \ldots . \tag{24b}$$

Consideration of the virtual work in any other panel element would have yielded an identical set of equations.

## 3. SOLUTION PROCEDURE

### 3.1. SOLUTION OF THE GOVERNING EQUATION

Equation (24) can be solved for the unknown coefficients $A_m$'s, from which coefficients $B_m$'s and $C_m$'s can be found using equations (12) and (13). The number of terms to be used in the calculation has to be decided after the convergence of the solution is verified. For an illustration purpose, we take the terms $m = -2, -1, 0, 1, 2$ in equation (24), which results in five equations for the five unknowns $A_{-2}, A_{-1}, A_0, A_{+1}, A_{+2}$. Then equation (24) can be put into a matrix equation

$$\begin{bmatrix} A1 & B1 & C1 & D1 & E1 \\ & F1 & G1 & H1 & I1 \\ & & J1 & K1 & L1 \\ & & & M1 & N1 \\ \text{Symmetric} & & & & O1 \end{bmatrix} \begin{Bmatrix} A_{-2} \\ A_{-1} \\ A_0 \\ A_1 \\ A_2 \end{Bmatrix} = \begin{Bmatrix} 0 \\ 0 \\ P1 \\ 0 \\ 0 \end{Bmatrix}, \tag{25}$$

where the matrix coefficients are

$$A1 = \left[D\left(\frac{\mu+2(-2)\pi}{L}\right)^4 - m_p\omega^2 + \frac{2\omega^2\rho_0 \mathrm{j}}{k_{y-2}}\right] + \frac{K_t}{L} - \frac{\omega^2 M}{L} + \frac{K_r}{L}\left(\frac{\mu+2(-2)\pi}{L}\right)^2,$$

$$B1 = \frac{K_t}{L} - \frac{\omega^2 M}{L} + \frac{K_r}{L}\left(\frac{\mu+2(-1)\pi}{L}\right)\left(\frac{\mu+2(-2)\pi}{L}\right),$$

$$C1 = \frac{K_t}{L} - \frac{\omega^2 M}{L} + \frac{K_r}{L}\left(\frac{\mu+2(0)\pi}{L}\right)\left(\frac{\mu+2(-2)\pi}{L}\right),$$

$$D1 = \frac{K_t}{L} - \frac{\omega^2 M}{L} + \frac{K_r}{L}\left(\frac{\mu+2(1)\pi}{L}\right)\left(\frac{\mu+2(-2)\pi}{L}\right),$$

$$E1 = \frac{K_t}{L} - \frac{\omega^2 M}{L} + \frac{K_r}{L}\left(\frac{\mu+2(2)\pi}{L}\right)\left(\frac{\mu+2(-2)\pi}{L}\right),$$

$$F1 = \left[D\left(\frac{\mu+2(-1)\pi}{L}\right)^4 - m_p\omega^2 + \frac{2\omega^2\rho_0 \mathrm{j}}{k_{y-1}}\right] + \frac{K_t}{L} - \frac{\omega^2 M}{L} + \frac{K_r}{L}\left(\frac{\mu+2(-1)\pi}{L}\right)^2,$$

$$G1 = \frac{K_t}{L} - \frac{\omega^2 M}{L} + \frac{K_r}{L}\left(\frac{\mu + 2(0)\pi}{L}\right)\left(\frac{\mu + 2(-1)\pi}{L}\right),$$

$$H1 = \frac{K_t}{L} - \frac{\omega^2 M}{L} + \frac{K_r}{L}\left(\frac{\mu + 2(1)\pi}{L}\right)\left(\frac{\mu + 2(-1)\pi}{L}\right),$$

$$I1 = \frac{K_t}{L} - \frac{\omega^2 M}{L} + \frac{K_r}{L}\left(\frac{\mu + 2(2)\pi}{L}\right)\left(\frac{\mu + 2(-1)\pi}{L}\right),$$

$$J1 = \left[D\left(\frac{\mu + 2(0)\pi}{L}\right)^4 - m_p\omega^2 + \frac{2\omega^2\rho_0 \mathrm{j}}{k_{y0}}\right] + \frac{K_t}{L} - \frac{\omega^2 M}{L} + \frac{K_r}{L}\left(\frac{\mu + 2(0)\pi}{L}\right)^2,$$

$$K1 = \frac{K_t}{L} - \frac{\omega^2 M}{L} + \frac{K_r}{L}\left(\frac{\mu + 2(1)\pi}{L}\right)\left(\frac{\mu + 2(0)\pi}{L}\right),$$

$$L1 = \frac{K_t}{L} - \frac{\omega^2 M}{L} + \frac{K_r}{L}\left(\frac{\mu + 2(2)\pi}{L}\right)\left(\frac{\mu + 2(0)\pi}{L}\right),$$

$$M1 = \left[D\left(\frac{\mu + 2(1)\pi}{L}\right)^4 - m_p\omega^2 + \frac{2\omega^2\rho_0 \mathrm{j}}{k_{y1}}\right] + \frac{K_t}{L} - \frac{\omega^2 M}{L} + \frac{K_r}{L}\left(\frac{\mu + 2(1)\pi}{L}\right)^2,$$

$$N1 = \frac{K_t}{L} - \frac{\omega^2 M}{L} + \frac{K_r}{L}\left(\frac{\mu + 2(2)\pi}{L}\right)\left(\frac{\mu + 2(1)\pi}{L}\right),$$

$$O1 = \left[D\left(\frac{\mu + 2(2)\pi}{L}\right)^4 - m_p\omega^2 + \frac{2\mathrm{j}\omega^2\rho_0}{k_{y2}}\right] + \frac{K_t}{L} - \frac{\omega^2 M}{L} + \frac{K_r}{L}\left(\frac{\mu + 2(2)\pi}{L}\right)^2,$$

$$P1 = \mathrm{j}2\omega\rho_0.$$

### 3.2. THE TRANSMISSION LOSS (TL) OBTAINED FROM THE SOLUTION

The power transmission coefficient that is a function of the angle of incidence ($\theta$) can be obtained as

$$\tau(\theta) = \left|\frac{I_t}{I_i}\right|, \tag{26}$$

where $I_i$ and $I_t$ are incident and transmitted normal intensities, respectively, and are given by

$$I_i = \frac{\omega\rho_0 k_{y0}}{2}, \quad I_t = \frac{\omega\rho_0}{2}\sum_{n=-\infty}^{\infty} |C_n|^2 \,\mathrm{Re}[k_{yn}]. \tag{27, 28}$$

The TL is defined as the logarithm of the inverse of the power transmission coefficient, which will depend on the incident angle. To estimate the TL for random incidences, the power transmission coefficient $\tau(\theta)$ is averaged to the Paris formula [22] to obtain the averaged coefficient $\bar{\tau}$:

$$\bar{\tau} = 2\int_0^{\theta_{lim}} \tau(\theta)\sin\theta\cos\theta\,\mathrm{d}\theta, \tag{29}$$

where $\theta_{lim}$ is the limiting angle above which it is assumed that no sound is incident upon the panel, which is taken as 72° as suggested by Mulholland *et al.* [23]. The actual integration of equation (29) was carried out numerically using the step size of 2°. The averaged TL is obtained as

$$TL_{avg} = 10 \log_{10}\left(\frac{1}{\bar{\tau}}\right). \tag{30}$$

The averaged TLs of the unstiffened and stiffened panels are compared in a narrow band format in Figure 2. The simulation conditions used to obtain Figure 2 are listed in Table 1. The unstiffened and stiffened panels, on which a plane wave is incident with an angle of 45°, are compared in terms of the TL in a narrowband format as shown in Figure 3. It is seen that the two TLs in Figures 2 and 3 show very similar characteristics. To save related computational work, a single incidence angle of 45° is used for subsequent analyses. Also, in Figures 2 and 3, the TLs calculated for the unstiffened panel are compared with those

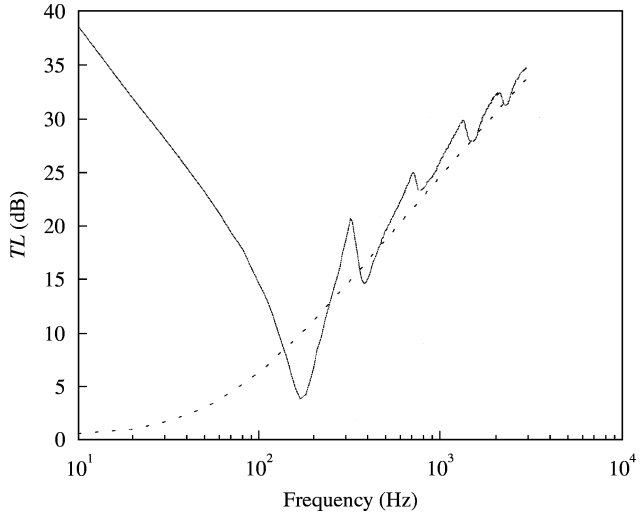


Figure 2. Comparison of the predicted averaged TLs between the stiffened and the unstiffened panels: ——, W/stiffener; -------, W/O stiffener.

TABLE 1

*Dimensions of the panel and simulation conditions*

| | | | | | |
|---|---|---|---|---|---|
| $K_t$ (N/m) | $3{\cdot}6 \times 10^9$ | $v$ | 0·33 | $L$ (mm) | 200 |
| $K_r$ (N m/rad) | 60 | $\rho$ (kg/m$^3$) | 2700 | $\psi$ | 1° |
| $E$ (Pa) | $7{\cdot}1 \times 10^{10}$ | $\rho_0$ (kg/m$^3$) | 1·21 | $c$ (m/s) | 343 |
| $h$ (mm) | 1·27 | $\theta$ | 0–72° | $\phi$ | 0° |
| $M$ (kg) | 0 | $\eta$ | 0·1 | $\omega/2\pi$ (Hz) | 10–3000 |

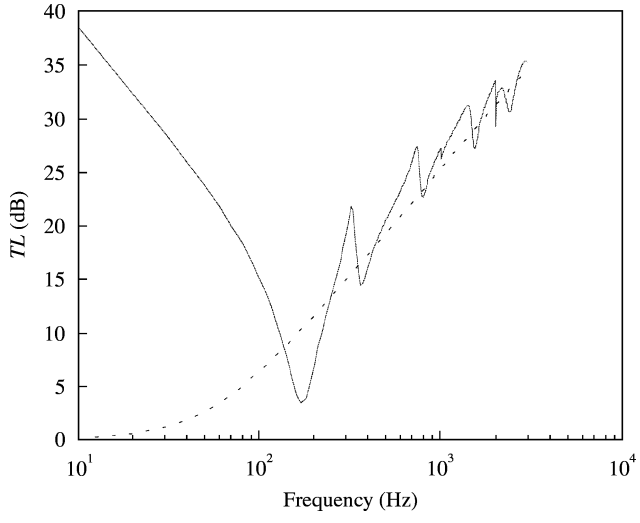


Figure 3. Comparison of the predicted TLs between the stiffened and the unstiffened panels on which a plane wave is incident with angle of 45°: ——, W/stiffener; -------, W/O stiffener.

obtained for the stiffened panel. It is seen that the effect of the stiffener is pronounced in the low-frequency range.

### 3.3. CONVERGENCE OF THE SOLUTION

Because the solutions are obtained in series forms, enough terms have to be used in the calculation to make the solutions converge. Once the solution converges at a given frequency, it can be assumed to converge for all frequencies lower than that. Therefore, the necessary number of terms is determined at the highest frequency of interest. A simple algorithm is used where the TLs are calculated at the highest frequency of interest, adding one term to the assumed expansion solution at a time. When the TLs calculated at two successive calculations are within a pre-set error bound (0·01 dB in this work), the solution is considered to have converged. The number of coefficients found in this way is used to calculate TL at all other frequencies below this highest frequency of interest.

Figure 4 shows as to how the calculated TL changes as the number of coefficients increases at the driving frequency of 3000 Hz. The same data shown in Table 1 is used for the stiffened panel but a single incidence angle of 30° is used. From the figure, 21 coefficients ($n = -10$ to 10) are enough to provide a converged solution at 3000 Hz.

## 4. PARAMETER STUDIES

The basic panel dimensions and simulation conditions used in the study are the same as those listed in Table 1, obviously, except for the parameter to be studied.

### 4.1. PARAMETERS RELATED TO MODELLING

#### 4.1.1. *Effect of the incidence angle*

The TLs calculated for three different incident angles (30, 45, 60°) are plotted in Figure 5, which indicates that the transmitted power slightly decreases (TL increases) with decreasing

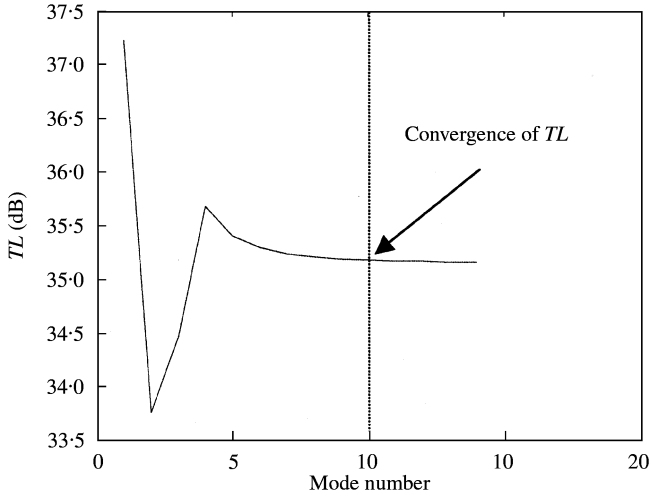


Figure 4. Coefficient covergence diagram for the stiffened panel ($t = 1{\cdot}27$ mm) at 3000 Hz.

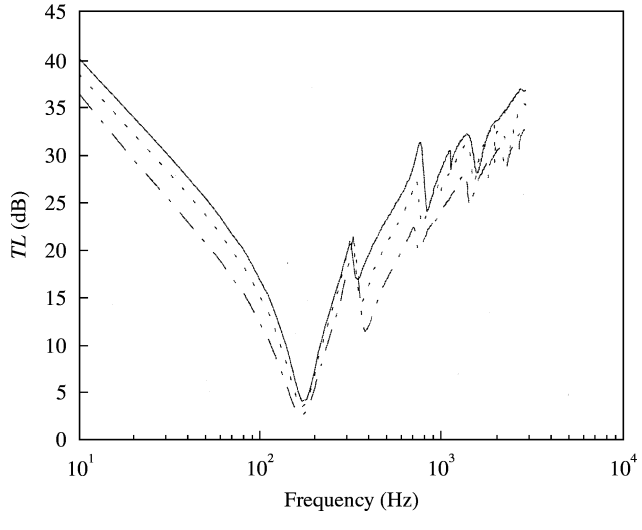


Figure 5. TL curves for the stiffened panel with respect to incidence angle: ——, 30°; -------, 45°; – · – · –, 60°.

incidence angle $\theta$. Because the qualitative aspect of the solution does not change for different angles, the incident angle of 45° is used for all subsequent calculations, which reduces the related computation time substantially.

### 4.1.2. *Effect of the phase attenuation*

Figure 6 compares the TLs calculated for three different phase attenuation parameters, 0°, 1° and 10°, which are chosen within a physically reasonable range. Notice that the choice of the phase attenuation coefficient influences the solution in a noticeable scale only in the low-frequency range, below 100 Hz in this case. The comparison suggests that the use of an arbitrarily small value for the attenuation angle will be acceptable for most purposes.

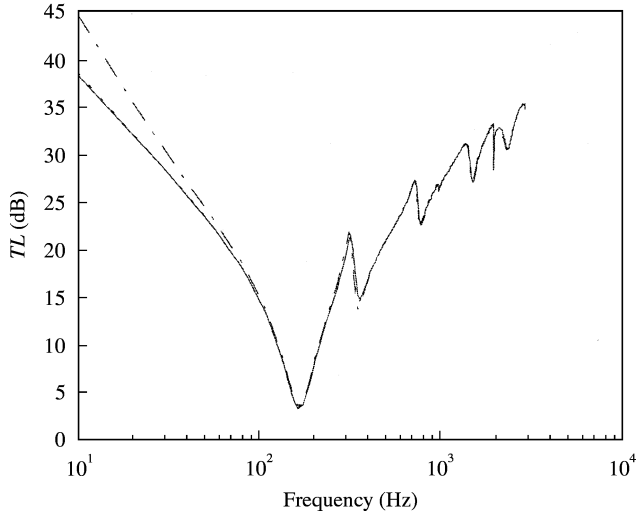


Figure 6. TL curves for the stiffened panel with respect to phase attenuation: ——, $\psi = 0°$; -------, $\psi = 1°$; –·–·–, $\psi = 10°$.

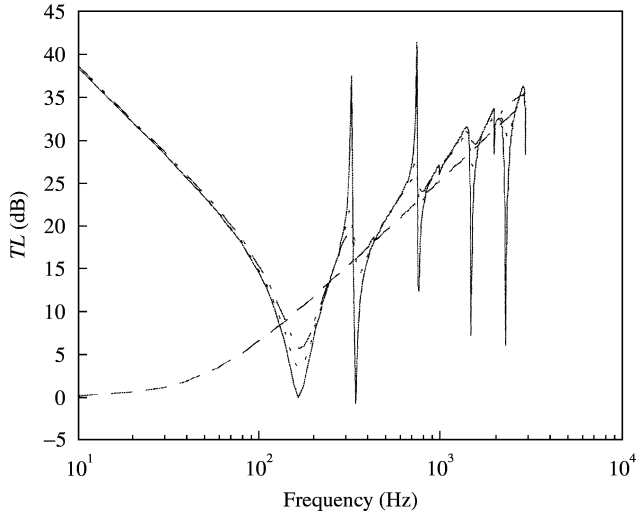


Figure 7. TL curves for the stiffened panel with respect to loss factor: ——, $\eta = 0$; -------, $\eta = 0{\cdot}1$; –·–·–, $\eta = 0{\cdot}2$; ————, W/O stiffener ($\eta = 0$).

Because the phase attenuation parameter $\psi$ is difficult to estimate, $1°$ is used as the angle in subsequent calculations.

### 4.1.3. *Loss factor*

The loss factor represents the structural damping of the panel, and is also difficult to estimate accurately. Figure 7 compares the TLs obtained for three loss factors for the stiffened panel and zero loss factor for the unstiffened panel. Figure 7 shows sound transmission loss curve, of the stiffened panel and of the unstiffened counterpart, in which the influence of damping can clearly be seen [24]. From the result, it can be inferred that

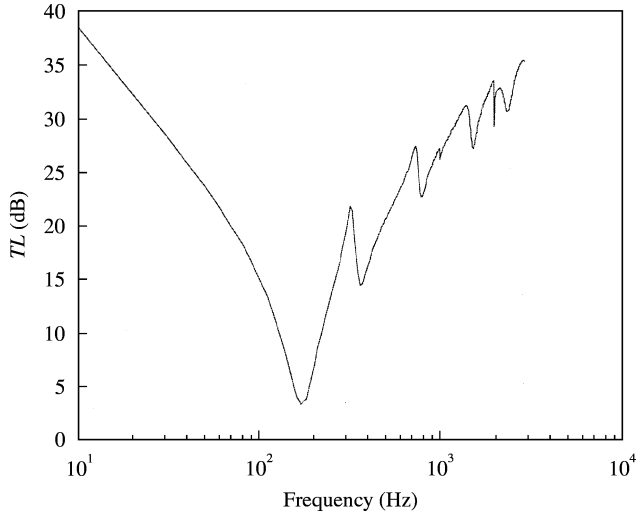


Figure 8. TL curves for the stiffened panel with respect to stiffener mass ($K_t = 3{\cdot}6 \times 10^9$ N/m): ——, 0%; -------, 10%; –·–·–, 100%; — — — —, 200%.

a damping treatment such as a coating is a good option for the stiffened panel to increase the TL in any significant scale. In all subsequent studies, 0·1 is used as the loss factor.

Notice that the effect of the stiffening features is detrimental to the sound transmission characteristics of the stiffened panel when compared with an unstiffened panel. One way of qualitatively understanding this feature is to consider that the wave reflection produced by the stiffeners changes the dispersion relationship in such a way that free waves having wave number components of supersonic phase velocity can propagate at frequencies below the unstiffened panel critical frequency, these components may cause the panel to be excited in a coincidental manner by incident sound waves at frequencies below critical. In practice, the effect on sound transmission is as though the critical frequency had been lowered by one or two octaves, the degree of change being dependent upon the spacing and stiffness (translational and rotational) of the stiffeners [24].

#### 4.1.4. *Stiffener mass effects*

TLs calculated when the stiffener has 0, 10, 100 and 200% of the mass of the panel are plotted in Figure 8. The figure indicates that the mass effect caused by the stiffener has virtually no influence on the TL in the case studied. Figure 9 shows the same comparison, using the TLs calculated for four different stiffener masses but reducing the translational stiffness of the stiffener drastically, from $K_t = 3{\cdot}6 \times 10^9$ to $1 \times 10^5$ N/m. This indicates that the stiffener mass has to be considered only when the translational spring is very soft, which is not a practical case. Generally, it is considered that the mass effect of the stiffener will not have to be considered in the analysis.

### 4.2. DESIGN PARAMETERS

#### 4.2.1. *Materials*

Figure 10 shows the effect of the material on the TL of the panel. Materials chosen for the comparison are steel, aluminum and brass as shown in Table 2. The figure shows that the TL of the brass is comparable with that of the steel in the middle frequencies ranging

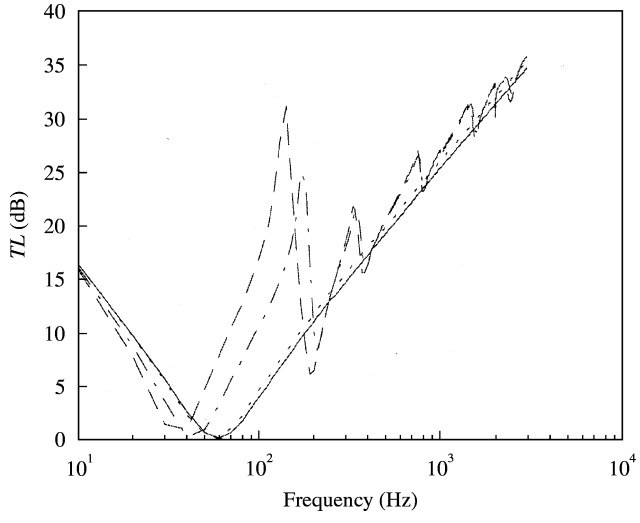


Figure 9. TL curves for the stiffened panel with respect to stiffener mass ($K_t = 1{\cdot}0 \times 10^5$ N/m): ——, 0%; -------, 10%; –·–·–, 100%; steel; – – – –, 200%.

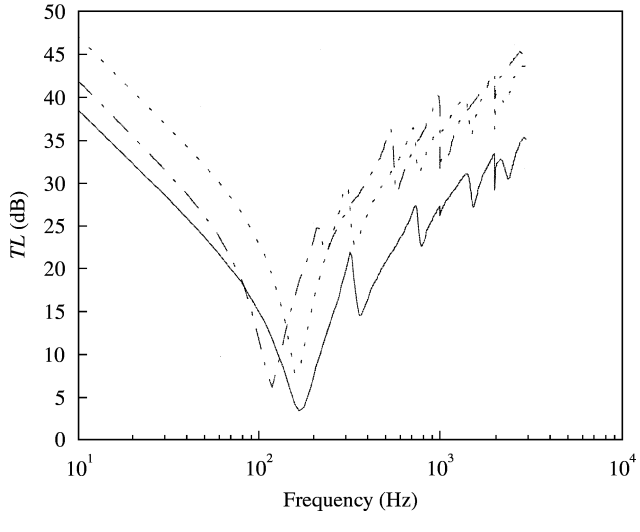


Figure 10. TL curves for the stiffened panel with respect to plate material: ——, aluminum; -------, steel; –·–·–, brass.

TABLE 2

*Material properties of the stiffened panel*

| | Steel | Aluminum | Brass |
|---|---|---|---|
| Density ($\rho$:kg/m$^3$) | 7750 | 2700 | 8500 |
| Young's modulus ($E$: Pa) | $1{\cdot}9 \times 10^{11}$ | $0{\cdot}71 \times 10^{11}$ | $1{\cdot}04 \times 10^{11}$ |
| The Poisson ratio ($v$) | 0·3 | 0·33 | 0·37 |

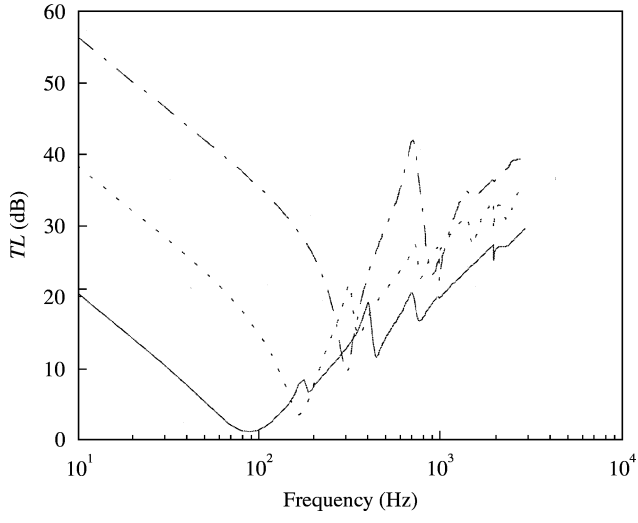


Figure 11. TL curves for the stiffened panel with respect to thickness of the panel: ——, $t = 0{\cdot}645$ mm; -------, $t = 1{\cdot}27$ mm; –·–·–, $t = 2{\cdot}54$ mm.

from 200 Hz to 2 kHz. Above 2 kHz, the brass will be the most effective material in the high-frequency range. This is as expected because the density of the brass is larger which makes it most effective in the mass-controlled high-frequency range. The figure also shows that aluminum, which has the lowest stiffness, is the least effective in the low-frequency range, which is again as expected because the low-frequency range is controlled by the stiffness. This type of comparison will be useful in practice when the basic design of a certain structure is to be decided.

### 4.2.2. *Panel thickness*

Figure 11 shows the effect of the panel thickness on the TL. Changing the thickness has a broadband effect on TL over the entire range of the frequency. In general, TL increases more in the low-frequency range, or the stiffness-controlled region, and less in the high-frequency range, or the mass-controlled region. As in the study on the effect of the stiffener, the structural enhancement is most effective in the low-frequency range. In the high-frequency range, other means such as the use of absorbing materials may be a more effective solution.

### 4.2.3. *Stiffener spacing*

As shown in Figure 12, smaller stiffener spacing increases the TL substantially in the low-frequency range, however, it obviously deteriorates the sound transmission in an overall sense. It can be qualitatively explained by considering that the panel consists of an assemblage of smaller panels. The transmission loss of small panels has been shown to be lower than that of the larger panels of the same material. Hence, the transmission loss of the unstiffened panel exceeds that of the assemblage. The stiffener spacing has to be determined by considering a tradeoff between an overall performance and sound transmission characteristics in the low-frequency range.

### 4.2.4. *Stiffness of the stiffener*

Figure 13 shows the effect of the rotational stiffness. The comparison was made for a very wide range of rotational stiffness, while the translational stiffness is set to zero. The figure suggests that the rotational spring has almost no influence on the sound transmission

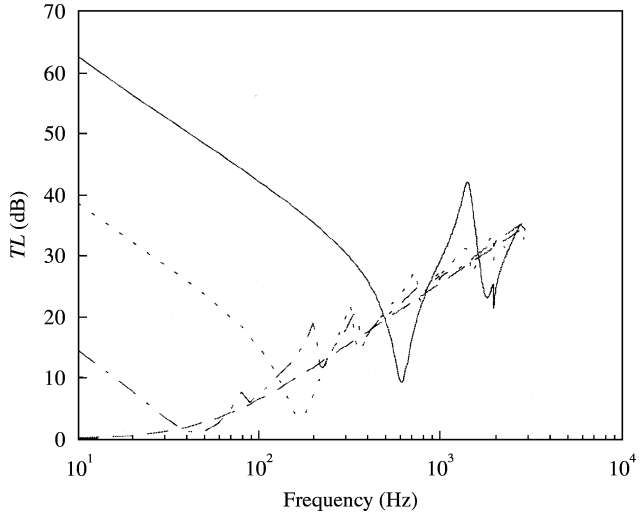


Figure 12. TL curves for the stiffened panel with respect to stiffener spacing: ——, $L = 100$ mm; -------, $L = 200$ mm; –·–·–, $L = 400$ mm; — — — —, W/O stiffener.

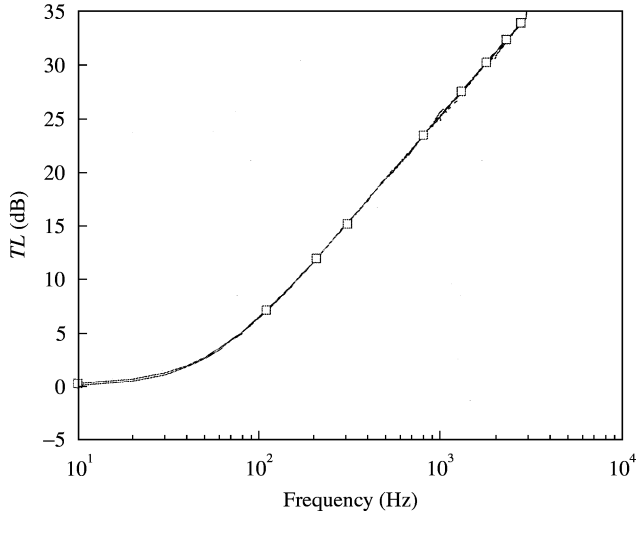


Figure 13. TL curves for the stiffened panel with respect to rotational stiffness of the stiffener: —□—, $K_r = 0$ N m/rad; ——, $K_r = 1{\cdot}2 \times 10^3$ N m/rad; -------, $K_r = 1{\cdot}2 \times 10^4$ N m/rad; —·—·—, $K_r = 1{\cdot}2 \times 10^5$ N m/rad.

except in the very low-frequency range. This is somewhat expected because the sound is induced by the transverse motion of the panel.

Figure 14 shows the effect of the translational spring stiffness when the stiffener spacing is $L = 200$ mm. As expected again, the effect is mostly in the low-frequency range. Also, the effect of the increase of this parameter becomes saturated after it exceeds a value that is enough to make the spring virtually a fixed support ($7{\cdot}1 \times 10^7$ N/m in this case).

## 5. CONCLUSIONS

An exact analysis procedure is developed to calculate the sound transmission through an infinitely long elastic panel stiffened only in one direction. The stiffener is modelled as a set

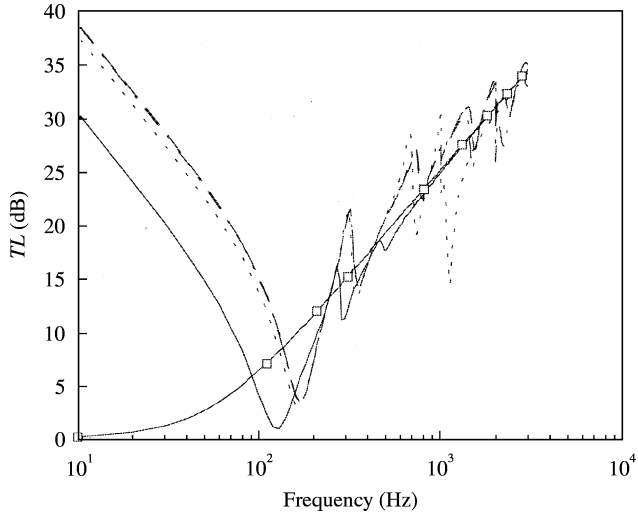


Figure 14. TL curves for the stiffened panel with respect to translational stiffness of the stiffener: —□—, $K_t = 0$ N/m; ——, $K_t = 7{\cdot}1 \times 10^5$ N/m; -------, $K_t = 7{\cdot}1 \times 10^6$ N m/rad; —·—·—, $K_t = 7{\cdot}1 \times 10^7$ N/m; $K_t = 3{\cdot}6 \times 10^9$ N/m.

of lumped mass, and rotational and translational stiffnesses attached to the panel. The dynamic equation that describes vibro-acoustic responses of the system is derived using the space harmonic approach and the virtual energy principle. The interaction between the stiffener and the panel, and the interaction between the panel and the acoustic media are fully considered in the derivation. A unique solution procedure is developed by relating the acoustic and structural space harmonic amplitudes utilizing the boundary conditions between the plate and the acoustic media. The solution is obtained as a truncated series of the assumed modes by solving a set of linear equations. A scheme to ensure the convergence of the solution is included in the solution procedure, therefore the series solution can be considered as the exact solution, which is considered to be the first exact analytical solution for this type of a problem.

Taking advantage of having an exact solution procedure, the performance of the stiffened panel as an acoustic barrier is studied in terms of the TL. Parameter studies are conducted for the parameters that a designer can practically choose, such as the panel material, stiffener spacing, size of the stiffener, and thickness of the stiffened panel. The parameter study also demonstrates the value of the analysis developed in this work as a design tool.

## ACKNOWLEDGMENT

The authors acknowledge the financial support by ArvinMeritor Industries related to this work.

## REFERENCES

1. D. J. MEAD and K. K. PUJARA 1971 *Journal of Sound and Vibration* **14**, 525–541. Space-harmonic analysis of periodically supported beams: response to convected random loading.
2. D. J. MEAD 1970 *Journal of Sound and Vibration* **11**, 181–197. Free wave propagation in periodically supported, infinite beams.

3. D. J. MEAD 1996 *Journal of Sound and Vibration* **190**, 495–524. Wave propagation in continuous periodic structures: research contributions from Southampton, 1964–1995.
4. Y. K. LIN 1960 *Journal of Applied Mechanics* **27**, 669. Free vibrations of continuous skin stringer panels.
5. Y. K. LIN 1962 *Journal of Aerospace Science* **29**, 67. Stresses in continuous skin-stiffened panels under random loading.
6. Y. K. LIN, I. D. BROWN and P. C. DELTSCHLE 1964 *Journal of Sound and Vibration* **1**, 14. Free vibrations of a finite row of continuous skin stringer panels.
7. C. A. MERCER 1965 *Journal of Sound and Vibration* **2**, 293. Response of a multi-supported beam to a random pressure filed.
8. M. HECKL 1964 *Journal of Acoustical Society of America* **36**, 1335. Investigations on the vibrations of grillages and other simple beam structure.
9. D. J. MEAD and E. M. WILBY 1971 *University of Southampton Report*. Forced vibration of periodically-supported beams subjected to convected, homogeneous pressure fields.
10. R. D. FORD 1962 *Ph.D. Thesis, University of Southampton*. The response of structures to jet noise.
11. C. A. MERCER and C. SEAVEY 1967 *Journal of Sound and Vibration* **6**, 149. Prediction of natural frequencies and normal modes of skin stringer panel rows.
12. G. P. MATHUR, B. N. TRAN, J. S. BOLTON and N.-M. SHIAU 1992 *Proceedings of* 14*th DGLR/AIAA Aeroacoustical Conference*, 102–105. Sound transmission through stiffened double-panel structures lined with elastic porous materials.
13. W. DESMET and P. SAS 1995 *Proceedings of First Joint CEAS/AIAA Aeroacoustical Conference* (16*th AIAA Aeroacoustics Conference*), AIAA-95-043, 311–320. Sound transmission of finite double-panel partitions with sound absorbing material and panel stiffeners.
14. E. H. DOWELL, C.-H. CHAO and D. B. BLISS 1977 *Journal of Sound and Vibration* **52**, 519–542. Acoustoelasticity: general theory, acoustic natural modes and forced response to sinusoidal excitation, including comparisons with experiments.
15. O. K. BEDAIR 1997 *Journal of Sound and Vibration* **199**, 87–106. Fundamental frequency determination of stiffened plates using sequential quadratic programming.
16. S. MUKHERJEE and S. PARTHAN 1995 *Journal of Sound and Vibration* **186**, 71–86. Wave propagation in one-dimensional multi-bay periodically supported panels under supersonic fluid flow.
17. J. WEI and M. PETYT 1997 *Journal of Sound and Vibration* **202**, 559–569. A method of analyzing finite periodic structures. Part 1: theory and examples.
18. J. WEI and M. PETYT 1997 *Journal of Sound and Vibration* **202**, 571–583. A method of analyzing finite periodic structures. Part 2: comparison with infinite periodic structure theory.
19. L. E. KINSLER, A. R. FREY, A. B. COPPENS and J. V. SANDERS 1982 *Fundamentals of Acoustics*. New York: John Wiley & Sons, Inc.
20. W. SOEDEL 1993 *Vibrations of Shells and Plates*. New York: Marcel Dekker, Inc.
21. L. CREMER, M. HECKL and E. E. UNGAR 1973 *Structure-Borne Sound*. Berlin: Springer-Verlag.
22. D. PIERCE 1981 *Acoustics*. New York: McGraw-Hill.
23. K. A. MULHOLLAND, H. D. PARBROOK and A. CUMMINGS 1967 *Journal of Sound and Vibration* **6**, 324–334. The transmission loss of double panels.
24. F. FAHY 2000 *Sound and Structural Vibration*. New York: Academic Press.